IOP Publishing

Turbulent Flows: an Introduction

Ian P Castro and Christina Vanderwel

Chapter 7

Internal wall-bounded flows

All the specific types of turbulent flow discussed in earlier chapters have been assumed to be remote from any solid walls. This chapter and the next explore the shear flows that directly result from the presence of a wall. Classic examples include turbulent pipe flow (an internal flow) and the turbulent boundary layer (an external flow). Such flows are necessarily more complex than the free shear flows discussed earlier, not least because sufficiently near to the wall, they must include significant viscous effects. The Reynolds number (however defined) thus almost always assumes greater importance than in the free shear flows discussed in chapter 6. After some initial remarks, we consider the major types of internal flow in sections 7.2 (Couette flows), 7.3 (channel flows), and 7.4 (pipe flows). External wall-bounded flows are considered in the next chapter (chapter 8). In all cases, the discussion starts with a brief consideration of the corresponding laminar flows. In the case of internal flows, these are among the very few exact solutions of the Navier–Stokes equations and set the scene for exploration of the turbulent versions which inevitably arise when the Reynolds number is high enough.

7.1 Initial remarks

Wall-bounded turbulent shear flows are exceedingly common, arguably much more common than the free shear flows discussed earlier. Internal flows through pipes and channels along with external flows around vehicles and over buildings are examples of flows in which mean flow shear is created in the boundary layer formed by the flow near the solid surface. In fact, the frictional effects near the wall provide the most common source of shear. Without these effects, there would be no turbulence. They arise as a result of *the no-slip condition* – the requirement that, because of nonzero viscosity, the velocity of the fluid at the wall must equal the wall's velocity (whether zero or not).

Consider, for example, the flow through a long pipe – an internal flow. One could reasonably claim, given the preponderance of pipes (and channels) of all sizes and in

doi:10.1088/978-0-7503-3619-2ch7

such numerous contexts, that this is *the* most common kind of fluid flow resulting from human endeavour. Indeed, the measurement of the flow rate in pipes might well be the most important measurement made daily and often continuously, throughout large sections of industry: an error of only a fraction of one percent could lead to the loss or gain of very large sums of money (for the supplier or the consumer). Recall section 2.8, which mentions Reynolds' early work on pipe flow. He showed that if the pipe Reynolds number exceeds a few thousand, the flow becomes fully turbulent. Most industrial pipework contains flows that have very much larger Reynolds numbers, so a large fraction of such flows are fully turbulent and thus, despite the extremely simple boundary conditions, not amenable to a full analytic solution. In addition, a crucial fact arising from the turbulent nature of such flows is that the power required to drive the flow through the pipe is usually orders of magnitude higher than would be needed if the flow remained laminar, as mentioned in section 1.3.

The planar equivalent of a pipe is a wide rectangular channel; figure 7.1 shows a snapshot of the fully turbulent flow in such a channel. We do not discuss the details here, but note that the flow typifies turbulence in that there are entangled eddy motions on a wide range of scales. It also typifies wall turbulence in particular, in that the eddy motions are of a much smaller scale nearest the wall than they are further away. Instantaneously, the cross-stream profile of the streamwise velocity is far from monotonic, reflecting the state of the flow at the instant the profile was obtained. This illustrates an important feature that we have not yet mentioned, perhaps because it should be self-evident (although it can be easily forgotten): the mean velocity profile in any turbulent flow *never* actually exists. Note, from the mean velocity profile shown in the figure, that the velocity gradient is at its largest at the two walls; the shear stress at the walls is much larger than it would be in laminar flow, emphasising the point made above, that much greater power is needed to drive the flow through the channel.

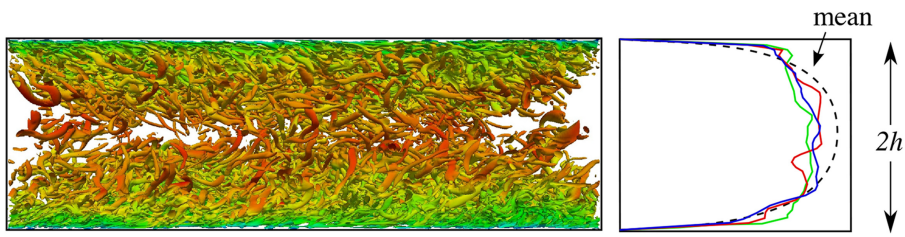

Figure 7.1. A snapshot of the eddy motions within a turbulent flow in a rectangular channel, visualised on the spanwise centreline, from a direct numerical simulation (DNS) at $\mathrm{Re}_\tau = 590$[1]. The direction of the flow is from left to right and the eddies are visualised using the Q criterion (see section 8.5) and are coloured according to the velocity magnitude – from green (lowest) to red (highest). On the right, there are three sample instantaneous profiles of the streamwise velocity, with the time-averaged (mean) profile shown as a dashed line.

[1] Reprinted from [19], copyright (2017) with permission from Elsevier.

7.2 Couette flows

7.2.1 The laminar case

Many of the laminar flows discussed in this section and the following sections will be familiar to readers who have studied basic fluid dynamics. The flows represent classical ones, for which the Navier–Stokes equations yield straightforward analytic solutions when the Reynolds number is low enough to prevent turbulence from arising. We include the fundamental results here, without needing to include much detail in the analysis, or extending the discussion to involve related alternative flows (laminar flow in branching channels or curved pipes, for example). Our purpose is merely to provide the background for an exploration of the corresponding turbulent flow. We begin by discussing Couette flow, a planar flow between two walls.

Figure 7.2 sketches the ideal cases reviewed here. They are contained in a rectangular channel of internal height $2h$ and width L_z. We assume its length, L_x, is very large compared with its other dimensions, so that the entry and exit regions of the duct, where the flow is still developing, can be ignored. Attention is thus focused on the 'fully developed' region in which the axial velocity does not (and cannot) depend on x and the flow is a simple one-dimensional one in which the velocity, $U(y)$, depends only on y. This assumes, of course, that $L_z/2h \ggg 1$, so that the influence of the side walls of the duct is negligible.

In the simplest version of this situation, one wall of the duct moves with a constant velocity, $U(y = 2h) = U_w$, say, for then no pressure gradient is needed to drive the flow – frictional forces at this upper wall suffice. Under these circumstances, the flow becomes a simple shear flow; the velocity between the upper and lower walls is given by $U/U_w = y/2h$. For the laminar case, the viscous shear stress, $\mu dU/dy$, is constant across the flow and obviously given by $\mu U_w/2h$. This is a Couette flow and is common in lubricating systems, often as the axisymmetric equivalent. U_w

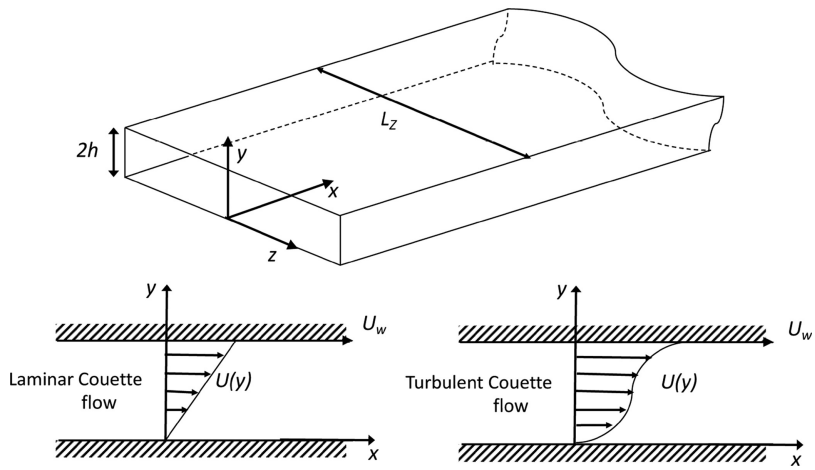

Figure 7.2. A long, straight, smooth-walled, rectangular channel with sketches of the characteristic velocity profiles for the cases of laminar and turbulent Couette flows (i.e. with a moving wall).

and h are the only pertinent velocity and length scales, respectively; therefore, as an appropriate Reynolds number for the flow, we can use either $\mathrm{Re}_w = U_w h/\nu$ or $\mathrm{Re}_c = U_c h/\nu$, (with the centreline velocity $U_c = 0.5U_w$). Once Re_w exceeds about 1200, the flow begins the transition to turbulence; see, for example, Aydin *et al* [3]. The transition process is not discussed here, and we now turn to consider the fully turbulent Couette flow.

7.2.2 The turbulent case

As in the laminar case, in the fully developed region there is no dependence on x and, provided $L_z/h \ggg 1$, there is no dependence on z either – the flow is essentially one-dimensional. The general mean momentum equation (2.16) is repeated here:

$$\frac{\partial U_i}{\partial t} + U_j\frac{\partial U_i}{\partial x_j} = -\frac{1}{\rho}\frac{\partial P}{\partial x_i} + \nu\frac{\partial^2 U_i}{\partial x_j \partial x_j} - \frac{\partial \overline{u_i' u_j'}}{\partial x_j}. \tag{7.1}$$

Note that the continuity equation directly implies that V must be zero all across the flow, because $\partial U/\partial x$ is zero and V is zero at the walls. (This is obviously true whether or not the flow is turbulent.) With the assumptions of no dependence on either x or z, the x-direction ($i = 1$) equation simplifies greatly and can then be integrated once to yield

$$\mu\frac{dU}{dy} - \rho\overline{u'v'} = \text{constant} = \tau_w, \tag{7.2}$$

where τ_w is the wall shear stress. Equation (7.2) is simply a statement that the total mean shear, the sum of the viscous and turbulence stresses, is constant across the flow. Since $\overline{u'v'}$ is zero at the walls, it is immediately clear that the mean velocity gradient cannot be constant across the whole flow, unlike in the laminar case summarised above. The velocity gradient at the walls is larger than it is elsewhere, and the mean velocity profile takes on a characteristic S-shape, as sketched in figure 7.2. In each near-wall region, viscous stresses are significant. At sufficiently high Reynolds numbers ($\mathrm{Re}_c = U_c h/\nu \ggg 1$), however, these viscous layers are thin and one might expect the central portion of the flow to approximate a steady version of the simple shear flow discussed in section 5.2 (but see below), for which the viscous stress in equation (7.2) is negligible and the turbulent shear stress is thus constant.

The viscous region is common to all wall-bounded flows and we explore it in more detail in the following section; it is sufficient to note here that it becomes thinner and thinner as the Reynolds number rises. Note immediately, however, that we can define a characteristic velocity scale of the near-wall flow by using the wall stress; thus, the *frictional velocity*, u_τ, is defined by $\rho u_\tau^2 = \tau_w$; U and y can be normalised as

$$U^+ = U/u_\tau \quad \text{and} \quad y^+ = yu_\tau/\nu, \tag{7.3}$$

respectively, so that equation (7.2) can be written as

$$\frac{dU^+}{dy^+} - \overline{u'v'}^+ = 1. \tag{7.4}$$

Now consider the origin of the turbulence. Recall from the earlier discussion of decaying homogeneous shear flow in section 5.2 that the only source of turbulence is the presence of the mean shear, so that there is a positive production term in the energy equation (5.29). For a fully developed, steady Couette flow, in which $dk/dt = 0$, the source of the shear stress in the central region ($-\overline{u'v'}$) must be a result of what happens at and near the two walls. This is intuitively obvious; in the absence of viscosity, the wall shear stress would be zero and whatever the velocity of the moving wall, no flow could be generated, as there would be no driving force.

This geometrically simple flow is perhaps the purest among the canonical wall-affected turbulent shear flows, not least because of its homogeneity in two space directions (x and z), the lack of any pressure gradient, and the absence of a gradient in shear stress. The flow is defined by only one parameter, the Reynolds number (in contrast to pipe flows, section 7.4, which have two controlling parameters). It has therefore been the study of numerous papers since it was first discussed by Couette in the late 1800s. But it is not, in fact, at all simple. The flow is fully turbulent above a Reynolds number (based on $U_w = 2U_c$ and the channel half-height, h) of a few thousand. Laboratory realisations of this pure, planar, flow are quite difficult to establish; they often involve a moving belt as the upper wall, which can be difficult to keep flat (at the speeds needed to establish a reasonably high Reynolds number) and to make long enough to ensure a fully developed region between the two ends. It is also usually necessary to initiate the flow in some way in order to ensure the correct mass flux. Reichardt [38] and Tillmark and Alfredsson [47, 48] are examples of early and more recent studies, respectively. To obviate the technical problems involved in setting up a truly planar flow, some laboratory studies have used the approximation provided by an annular flow in a narrow channel between two long concentric cylinders, with either the inner or outer cylinder rotating at a fixed speed. If the gap between the cylinders, g, say, is sufficiently small compared to their circumference, L_c, say, the annular flow is closely planar. There are hundreds of papers in this category, starting, perhaps, with the classical works of G I Taylor [45, 46], but nearly all of them are not concerned so much with the nature of a pure turbulent Couette flow as with the details of the transitional processes that occur once the Reynolds number is high enough. Actually, even for very large L_c/g, the influence of the well-studied secondary flows that occur prior to transition and continue beyond it (including the classic Taylor vortices) can never really allow this situation to be a genuine surrogate for a true planar Couette flow.

One might think that it would be easier these days to study the flow using DNS and, in some ways, this is true. However, this approach is not without difficulty because of the very long and wide structures that are present in the flow [17]; this makes the problem significantly more expensive than obtaining the DNS solutions for a Poiseuille (pipe) flow at comparable Reynolds numbers. Nonetheless, a number of DNS results are now available; figure 7.3 shows some results from the study of Avsarkisov *et al* [2]. We use these as being sufficiently typical to make a number of basic points about turbulent Couette flow without delving into great detail. Note,

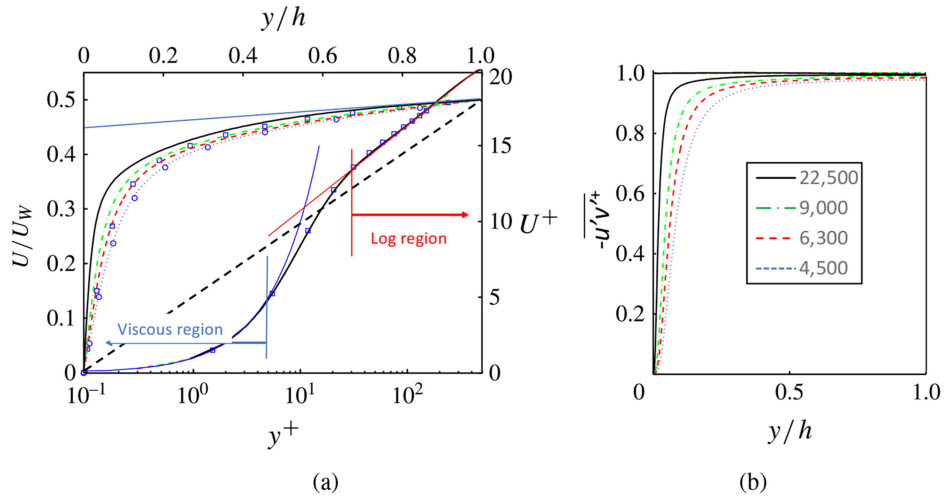

Figure 7.3. (a) Mean velocity profiles of plane Couette flows at various Reynolds numbers, over one half of the channel and normalised using the outer (top, left: h, U_w) and inner (bottom, right: ν/u_τ, u_τ) scales. (b) The turbulent shear stress. $\mathrm{Re}_w = hU_w/\nu$ values are shown in the legend. In (a) the straight, dashed black line represents the laminar profile (U/U_w versus y/h), the lower black line illustrates the same data as those shown by the upper black line but plotted using inner scaling, the solid blue line depicts the viscous law, $U^+ = y^+$, and the solid red line shows $U^+ = 1/\kappa \ln(y^+) + B$ with $\kappa = 0.41$, $B = 5.1$. The straight blue line at the top indicates the gradient of U/U_w at $y/h = 1$. The symbols are for other sets of computations at comparable Re_c, as detailed in [2]. Only one half of the channel, with a width of $2h$, is shown; the other half of the mean flow consists of an inverted mirror image, with U/U_w rising to unity at the moving wall ($y/2h = 1$)[2].

incidentally, that since the sum of the normalised viscous and Reynolds shear stresses is necessarily unity for all Reynolds numbers, as required by equation (7.4), figure 7.3 does not include the former; the frictional stress, dU^+/dy^+, is simply the difference between unity and the Reynolds shear stress data.

First, as mentioned above, the frictional layer near the wall ($y/h = 0$) becomes thinner as the Reynolds number rises. This is obvious in figure 7.3(a) from the increasingly full mean velocity profile in outer scaling (i.e. U/U_w versus y/h) and, in figure 7.3(b), from the reducing region in which the frictional shear stress is significant. Second, notice how much larger the velocity gradient near the wall is in the turbulent case, compared with the laminar case, emphasising the much larger wall stress very close to the wall and thus the much greater drag when turbulent flow occurs. It is straightforward to show that the turbulent to laminar wall stress ratio is given by $2\mathrm{Re}_\tau/(U^+|_{y=h})$, where $\mathrm{Re}_\tau = u_\tau h/\nu$; for the data in the figure at $\mathrm{Re}_c = 22500$ ($\mathrm{Re}_\tau = 550$), the ratio is about 55. Third, recall that we might have anticipated a central region of uniform velocity gradient (shear) in which the flow is similar to homogeneous shear flow (a steady version of the homogeneous shear flow turbulence (HSFT) discussed in section 5.2). Figure 7.3(a) suggests that if there is a region of constant shear, its strength weakens with increasing Reynolds number and at $\mathrm{Re}_c = 22500$ it is given by $d(U/U_w)/d(y/h)|_{y/h=1} \approx 0.1$, shown as the thin blue line at

[2] Reproduced with permission from [2], copyright Cambridge University Press.

the top of the figure. It appears to be an open question whether this shear tends towards zero at an infinite Reynolds number [22] or to some small finite value [8]. What is clear, however, is that the reduction in shear is quite slow as Re_w rises.

7.2.3 The viscous sublayer

Consider now the mean velocity profile of figure 7.3(a) plotted as U^+ versus y^+. It was Prandtl [37] who first postulated that at high Reynolds numbers, there is an inner layer close to the wall, in which the mean velocity profile must be determined only by viscous scales – independently of the characteristic length and velocity scales far away from the wall – in this case, h and U_w. The natural velocity scale in the viscosity-dominated region is u_τ (as mentioned earlier) and the viscous length scale, which we call η_v, must then be $\eta_v = \nu/u_\tau$. Note that this is quite distinct from the Kolmogorov scale, η, discussed in section 3.3. Hence, $y^+ = y/\eta_v = yu_\tau/\nu$ is a wall distance appropriately normalised by this viscous scale, as previously expressed in equation (7.3). It can be thought of as a local Reynolds number, so its magnitude at any point is a measure of the relative importance of the viscous and turbulent processes. U^+ ($=U/u_\tau$) and y^+ are normally thought of as the velocity and the wall distance in *wall units* (i.e. *inner scaling*). It is clear that in the region very close to the wall, where the turbulence shear stress $\overline{u'v'}$ can be ignored when compared to the viscous stress, equation (7.2) leads directly to

$$U^+ = y^+. \tag{7.5}$$

This viscosity-dominated region is usually called the *viscous sublayer*, although sometimes it is referred to as the laminar sublayer – rather a misnomer, as that could suggest there are no velocity fluctuations within it, which is not true. Figure 7.3(a) includes the sublayer $U^+ = y^+$ relation and it can be seen to describe the profile up to $y^+ \approx 5$. Note that equation (7.5) is not exact; a fuller analysis shows that $U^+ = y^+$ is correct up to $\mathcal{O}(y^{+4})$ (i.e. a Taylor series expansion shows, on applying the boundary conditions, that near the wall terms in y^{+2} and y^{+3} are identically zero, see Pope [36], for example). Notice, too, how thin the viscous sublayer is; at $y^+ = 5$, $y/h < 1\%$, emphasising how taxing it is to undertake a laboratory experiment to measure velocities within this viscous region, which becomes increasingly thin as the Reynolds number rises.

7.2.4 Beyond the viscous sublayer

Further from the wall, the turbulence shear stress begins to be significant and eventually, after a region usually called the *buffer layer*, the profile appears to follow a log-linear relation, above around $y^+ = 30$, which can be written

$$U^+ = A \ln(y^+) + B. \tag{7.6}$$

The reasons for which one might expect such a profile are explained in section 7.3.2.

One of the practically important measures related to the energy needed to drive the flow in any wall-bounded situation (or, equivalently, the drag the flow imposes on the surface) is what is called the *skin friction coefficient*, which can be defined (for this Couette flow) in terms of the wall velocity U_w by

$$C_f = \frac{\tau_w}{\rho U_w^2/2} = 2\left(\frac{u_\tau}{U_w}\right)^2. \tag{7.7}$$

If equation (7.6) holds all the way to the centre of the channel (where $U^+ = U_w^+/2$), it follows that

$$C_f = 0.5/(A\ln(\mathrm{Re}_\tau) + B)^2, \tag{7.8}$$

showing that C_f falls with increasing Re_τ, but much more slowly than it would in the laminar Couette flow, for which $C_f = 1/\mathrm{Re}_w = 1/(2\mathrm{Re}_\tau^2)$. So, for example, taking $A = 2.5$ and $B = 5$ as typical for equation (7.5), the ratio of turbulent to laminar friction coefficients (if the flow were somehow to remain laminar) is about 11 at $\mathrm{Re}_\tau = 50$ but about 1330 at $\mathrm{Re}_\tau = 500$.

7.2.5 The turbulence

Finally, we make a few comments about the nature of the turbulence away from the wall region. We show first, in figure 7.4(a), profiles across the channel of the three normal Reynolds stresses (as rms values in viscous units, i.e. normalised by u_τ). Note first that there is a maximum in u'^+_{rms} of around 2.8 close to the wall, which turns out to be fairly typical of wall-bounded flows. Second, because the turbulence kinetic energy production term is nonzero across the whole flow, there is significant axial stress at the centreline – $u'^+_{\mathrm{rms}} \approx 2.1$. Third, it is clear that the turbulence is anisotropic throughout the flow, including around the centreline – much more so than in pure channel flow, see section 7.3.

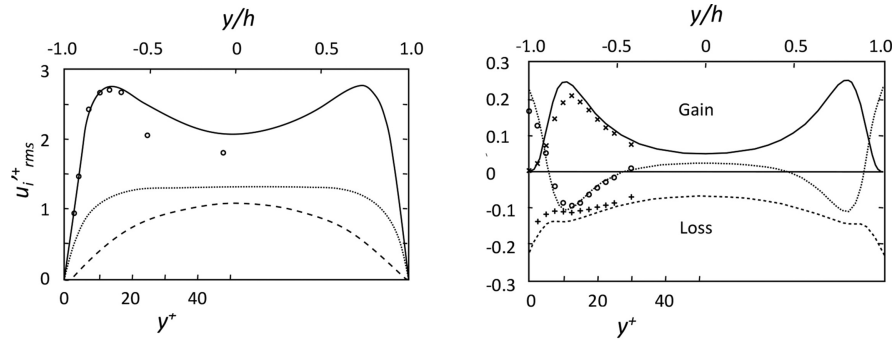

Figure 7.4. DNS data for a Couette flow at $\mathrm{Re}_\tau = 52$ from [18]. (a) normalised root-mean-square velocity fluctuations; solid line, u'^+_{rms}; dashed line, v'^+_{rms}; dotted line, w'^+_{rms}. Symbols are laboratory data at $\mathrm{Re}_\tau = 82$ from [5]. (b) Turbulent kinetic energy budget. Solid line, production; dashed line, dissipation; dotted line, transport. Symbols are from a DNS of channel flow at $\mathrm{Re}_\tau = 180$ [23][3].

[3] Reproduced with permission from [18], copyright Cambridge University Press.

The turbulent kinetic energy equation and the Reynolds stress equations are not exactly those presented and discussed in section 5.2, for in that case of homogeneous isotropic shear flow we assumed initial homogeneity in the turbulence and, because the velocity gradient dU/dy is invariable with y, the homogeneity remains for all time (refer to the argument just prior to equation (5.29)). However, in the case of Couette flow, although there may be a region of closely constant velocity gradient in the centre, it is certainly not constant across the whole flow. This leads to the appearance of an additional term in the Reynolds stress equation, which, for steady flow, from equation (2.27), becomes (recalling $V = W = 0$, $\partial/\partial x = \partial/\partial z = 0$)

$$\begin{aligned} 0 \quad = \quad & -\overline{u_i' u_j'}\frac{dU}{dy} - \overline{\frac{p'}{\rho}\left(\frac{\partial u_i'}{\partial x_j} + \frac{\partial u_j'}{\partial x_i}\right)} - \frac{\partial}{\partial y}\left(\overline{u_i' u_j' v'} + \overline{\frac{p' u_j'}{\rho}}\delta_{i2} + \overline{\frac{p' u_i'}{\rho}}\delta_{j2}\right) \\ & - 2\nu\overline{\frac{\partial u_i'}{\partial x_k}\frac{\partial u_j'}{\partial x_k}}. \end{aligned} \tag{7.9}$$

So, for example, with $i = j = 1$ (in equation (2.27), for the $\overline{u'^2}$ stress), the equation describing the transport of the streamwise component of the turbulence energy, $\frac{1}{2}\overline{u'^2}$, is

$$0 = -\overline{u'v'}\frac{dU}{dy} - \frac{1}{2}\frac{\partial}{\partial y}\overline{u'^2 v'} + \overline{\frac{p'}{\rho}\frac{\partial u'}{\partial x}} - \frac{1}{3}\epsilon, \tag{7.10}$$

which, compared with equation (5.36) for homogeneous shear flow, includes the triple-velocity-product term which would be zero if the turbulence were homogeneous. Nonetheless, DNS experiments have shown that this term is, in fact, very small except close to the wall. This equation for the axial Reynolds stress is the only one that contains the mean velocity gradient (i.e. a nonzero energy production term), so the mean flow drives the production of $\overline{u'^2}$. Energy in the other normal stress components arises as a result of the pressure strain terms (as discussed in section 5.2.2) but also, in this case, the nonzero triple-velocity-product turbulence transport. The kinetic energy equation (obtained by summing the three normal stress equations) is

$$0 = -\overline{u'v'}\frac{dU}{dy} + \frac{d}{dy}\overline{kv} + \frac{1}{\rho}\frac{d}{dy}\overline{p'v'} - \epsilon. \tag{7.11}$$

This shows directly that the imbalance between the production and dissipation of turbulence kinetic energy (k) at any point in the flow – the first and last terms – is a direct consequence of the transport of energy in the y direction. Even when the triple product term is close to zero, the pressure–velocity transport of k is not. Figure 7.3 (b) shows the turbulence kinetic energy balance for the same Couette flow (in which the fluctuation velocities are those shown in figure 7.3(a)). It is clear that the transport terms (the central two terms in the above equation, plus the viscous diffusion) is significant close to the walls, where there is thus no balance between production (the first term) and dissipation (the final term). In fact, as $y^+ \to 0$, the

balance is essentially one between the inward transport of k and dissipation. Even in the central part, however, the transport term remains significantly nonzero.

We emphasise that equations (7.9)–(7.11) are written without the viscous diffusion terms, on the assumption that they are negligible. However, although at high enough Reynolds numbers this is not unreasonable in the central part of the flow, very near the wall, viscous diffusion unsurprisingly plays a significant role at any Reynolds number. In fact, it has been shown through detailed DNS studies [2] that for y^+ below about five (i.e. within the viscous sublayer), the missing viscous term in equation (7.9) balances dissipation, and all other terms are negligible. The same is true for the transport equation for $\overline{w'^2}^+$. This is reflected in the transport term shown in figure 7.4(b), which clearly becomes comparable (but of opposite sign) to dissipation below about $y^+ = 5$; this is because of the relatively large viscous diffusion, which is much larger than the other transport terms, although it is not separated from these in the figure. On the other hand, for $\overline{v'^2}^+$ the balance in that region is between pressure strain and turbulent (triple product) transport, and for $\overline{u'v'}^+$ the balance is between pressure strain and pressure diffusion. Clearly, fully developed turbulent Couette flow is complex, despite the fact that it is the flow with the simplest possible boundary conditions and, unlike all other wall flows, dependent on only one free parameter – the Reynolds number (Re_c, say).

Incidentally, since equation (7.4) shows that, at the centreline, the Reynolds shear stress, $-\overline{u'v'}^+$, is $(1 - dU^+/dy^+|_{y=h})$, the turbulence kinetic energy production there can be written as

$$P_{y=h} = \left.\frac{dU^+}{dy^+}\right|_{y=h} \left(1 - \left.\frac{dU^+}{dy^+}\right|_{y=h}\right). \tag{7.12}$$

This rather remarkable result is exact for all Couette flows and is independent of the Reynolds number. For the case shown in figure 7.3, for which the normalised velocity gradient at the centreline is about 0.05, the turbulence production on the centreline is thus about 0.048, which corresponds to the DNS result.

Overall, whilst the various turbulence statistics discussed above do depend on the Reynolds number to a greater or lesser extent, the general behaviour is similar in many respects to that for the more common case of pure channel flow, which we now discuss. Readers wishing to pursue the topic of Couette flows in more detail could refer, for example, to the joint experimental and numerical studies of Bech [5] and the DNS studies of Komminaho *et al* [18] and Tsukahara *et al* [50] and the references therein.

7.3 Channel flows

7.3.1 Governing equations

Channel flows, like Couette flows, occur between two flat plates that form a duct, see figure 7.5. The simplest case is that in which neither duct wall moves, so that the flow is driven solely by an applied streamwise pressure gradient. There are more

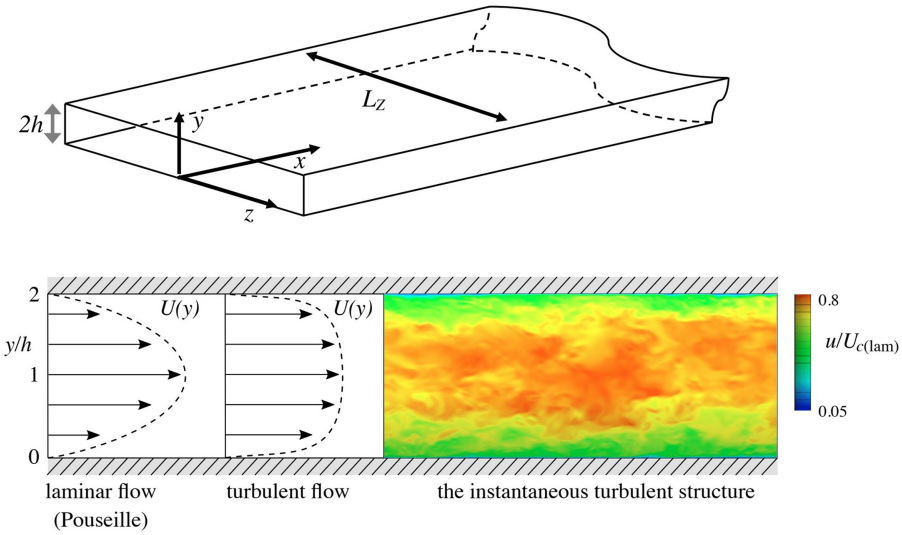

Figure 7.5. Sketch of the channel geometry, the laminar and turbulent velocity profiles in plane channel (left) and a snapshot from a numerical computation of the flow at $\mathrm{Re}\tau = 930$, from a video by J Lee[4]. Dark green denotes the lower velocities, shading towards red for the highest. The disorganised nature typical of turbulent flows is apparent.

complicated cases in which a pressure gradient is applied and, simultaneously, one wall moves relative to the other, but we do not consider such cases. For a laminar flow and fixed walls, consideration of the streamwise momentum equation, or a simple force balance argument, lead to a parabolic velocity profile given by

$$\frac{U}{U_m} = 2\frac{y}{h}\left(1 - \frac{y}{2h}\right), \tag{7.13}$$

where the maximum velocity on the channel centreline, U_m is $(h^2/2\mu)(dP/dx)$.

At high enough Reynolds numbers, the flow becomes transitional, and we now move on to a discussion of the fully developed turbulent channel flow. Figure 7.5 shows the geometry, a sketch of the mean velocity profile under laminar and turbulent conditions, and a snapshot from a DNS computation of the turbulent flow.

As in Couette flows, away from the entry and exit regions of a fixed-wall channel flow, i.e. in the fully developed region, the velocity statistics do not depend on x, nor, for wide enough channels and away from the side walls, on z. The flow is therefore statistically stationary and one-dimensional, just as in Couette flows. Since the flow is symmetric about the channel centreline, the statistics at y are identical to those at $2h - y$ and, in discussing the flow, we can simply consider the lower half, i.e. between $y = 0$ and $y = h$ – see figure 7.1. Defining the bulk velocity, U_B, as

[4] https://www.youtube.com/watch?v=t_5tEqa8rYs&ab_channel=jinLEE, courtesy of Hyung Jin Sung.

$$U_B = \frac{1}{h}\int_0^h U dy, \tag{7.14}$$

an appropriate Reynolds number is given by $\mathrm{Re}_B = U_B h/\nu$. It is known that the flow becomes fully turbulent once $\mathrm{Re}_B > 900$. As in Couette flow, we can consider the mean axial momentum equation or a simple force balance over the whole flow, in order to deduce how the shear stress varies. The three mean momentum equations (2.16) simplify to

$$0 = -\frac{1}{\rho}\frac{\partial P}{\partial x} - \frac{\partial \overline{u'v'}}{\partial y} + \nu\frac{\partial^2 U}{\partial y^2}, \tag{7.15}$$

$$0 = -\frac{1}{\rho}\frac{\partial P}{\partial y} - \frac{\partial \overline{v'^2}}{\partial y} \tag{7.16}$$

and

$$0 = -\frac{1}{\rho}\frac{\partial P}{\partial z}. \tag{7.17}$$

Note that continuity is automatically satisfied. These equations differ from their laminar equivalents by the appearance of the usual turbulent stress terms in equations (7.15) and (7.16), and they differ from the turbulent Couette flow because of the nonzero streamwise pressure gradient. P is clearly independent of z, and based on equation (7.16), its variation across the channel is a second-order effect:

$$\rho\overline{v'^2} + P = P_w(x), \tag{7.18}$$

where P_w is the mean pressure at the walls and depends only on x. Substituting this result into equation (7.15) yields

$$\left(\frac{\mathrm{d}P_w}{\mathrm{d}x}=\right)\frac{\mathrm{d}P}{\mathrm{d}x} = \frac{\mathrm{d}\tau}{\mathrm{d}y}, \tag{7.19}$$

where the total shear stress, τ, is given by

$$\tau = \mu\frac{\mathrm{d}U}{\mathrm{d}y} - \rho\overline{u'v'}. \tag{7.20}$$

The axial pressure gradient is, of course, what drives the flow; it acts to balance the wall stresses. Unlike the case of Couette flow, τ is clearly not constant with y. However, both sides of equation (7.19) must be constant (since one side is a function of y only and the other is a function of x only) so, using the boundary conditions, it follows that

$$\tau(y) = \tau_w\left(1 - \frac{y}{h}\right) \tag{7.21}$$

and also that

$$-\frac{\mathrm{d}P_w}{\mathrm{d}x} = \frac{\tau_w}{h}, \tag{7.22}$$

where τ_w is the wall stress (at $y = 0$). It is therefore the shear stress *gradient*, rather than the shear stress itself, that is constant across the whole channel. This is true whether or not the flow is turbulent and, in the laminar case, it is equations (7.21) and (7.22) that lead to the parabolic velocity profile quoted in equation (7.13). This laminar case is usually known as Poiseuille flow (as is the corresponding pipe flow case discussed in section 7.4), although some authors also refer to the turbulent channel case as a Poiseuille flow, despite the fact that it does not have a parabolic velocity profile.

7.3.2 The mean velocity profile

On dimensional grounds, the mean velocity gradient can depend on only two independent groups, y/h and Re. We can therefore write

$$\frac{\mathrm{d}U}{\mathrm{d}y} = \frac{u_\tau}{y}\Phi\left(\frac{y}{h}, \frac{y}{\eta_v}\right), \tag{7.23}$$

where η_v is the viscous length scale defined in section 7.2.3 as ν/u_τ. Near enough to the walls (i.e. when $y/h \ll 1$), recall that Prandtl postulated that only the viscous scales are important and the wall units are defined by equation (7.3), so that equation (7.23) must become

$$\frac{\mathrm{d}U}{\mathrm{d}y} = \frac{u_\tau}{y}\Phi_i\left(\frac{y}{\eta_v}\right) \quad \text{for} \quad \frac{y}{h} \ll 1. \tag{7.24}$$

Using wall scaling (i.e. equation (7.3), $y^+ = y/\eta_v = yu_\tau/\nu$ and $U^+ = U/u_\tau$), this becomes

$$\frac{\mathrm{d}U^+}{\mathrm{d}y^+} = \frac{1}{y^+}\Phi_i(y^+) \tag{7.25}$$

which integrates to

$$U^+ = f(y^+). \tag{7.26}$$

(As in Couette flow, in the viscosity-dominated region, this is just $U^+ = y^+ + \mathcal{O}(y^{+4})$.) In this near-wall region, we can write

$$y^+\frac{\mathrm{d}U^+}{\mathrm{d}y^+} = \Phi_i(y^+) = y^+f'(y^+). \tag{7.27}$$

Now suppose that the Reynolds number is sufficiently large that there is a region well outside the viscous sublayer in which viscosity is irrelevant but y is still much less than h. Then Φ_i in equation (7.24) must be constant; we will call this constant $1/\kappa$ and call κ the *von Kármán constant*, so that integration yields

$$U^+ = \frac{1}{\kappa}\ln(y^+) + A. \tag{7.28}$$

This is the celebrated logarithmic *law of the wall* (commonly called the *log law*) which von Kármán first deduced in 1930; it can be thought of as one of the few exact results in turbulence, although we emphasise that it is only true asymptotically as $\mathrm{Re}\to\infty$. It requires the existence of a region in which y is large compared to η_v but small compared to h; this region is often called the *inertial layer* and sometimes the 'overlap' region. There are various alternative arguments that lead to this result but, in some ways, the above approach is the most satisfying, since it depends on minimal assumptions.

In the region beyond the viscous wall layer, one also expects that the departure of the mean velocity from its centreline value, i.e. $U_c - U(y)$, will be independent of viscosity and that the appropriate length scale will thus be h rather than η_v. Classically, the velocity scale appropriate to this velocity deficit in the outer region is still u_τ, for to an observer on the centreline and moving at the centreline velocity, the only effect of the wall is to transmit a shear stress, τ_w. (Arguments for an alternative velocity scale have been proposed but are not discussed further here.) This all implies that

$$U_c^+ - U^+(y) = g(y/h), \tag{7.29}$$

which is usually called the *velocity defect law*, and we can write the Φ in equation (7.23) as $\Phi_o(y/h)$. It follows that

$$y^+\frac{\mathrm{d}U^+}{\mathrm{d}y^+} = \Phi_o\left(\frac{y}{h}\right) = -\frac{y}{h}g'\left(\frac{y}{h}\right). \tag{7.30}$$

Since y^+ and y/h are independent variables, this equation and equation (7.27) together require that $\Phi_o = \Phi_i$. After the integration of equation (7.30) between the limits y and h and (for velocity) U^+ and U_c^+, we can express the defect velocity as

$$U_c^+ - U^+ = -\frac{1}{\kappa}\ln\left(\frac{y}{h}\right) + B. \tag{7.31}$$

It is worth noting that in recent decades there has been some (often heated!) discussion about whether the log law, equation (7.28), is, in fact, the most appropriate relationship for the velocity profile outside the viscous wall region. The alternative is to take it as a power law (extending well above the inertial layer), i.e. $U^+ = ay^{+n}$, where a and n are functions of the Reynolds number. This often results from an alternative assumption about the appropriate velocity scale to use for the outer flow. Interested readers might like to consult, for example, the discussion presented in [7]. Nonetheless, the weight of experimental evidence, both from laboratories and computer simulations, is, in our view, strong enough to provide powerful evidence for the efficacy of the log law in an inertial layer, although one must always bear in mind that theoretically it is only an asymptotic result requiring a sufficiently large Reynolds number.

7.3.3 Some data and their implications

We now present some experimental confirmation of the log law. First, figure 7.6 shows profiles from the laboratory channel flow experiment of Wei and Willmarth [52], undertaken in the 1980s, in which (almost for the first time) laser Doppler anemometry (LDA) was used to obtain the data, which avoids the difficulties associated with using hot-wire probes within the channel. (In retrospect, these difficulties were evident in a number of earlier studies, not least the early work of Laufer [20], and especially in the near-wall region.) The experiments also covered a wider range of Reynolds number ($\mathrm{Re}_c = hU_c/\nu$) than most previous studies – a factor in excess of 13. In figure 7.6(a), the various regions of the flow are indicated and it is clear that the data yield a reasonable collapse to a log law above the buffer layer. (Although, in principle, the authors could have used the known channel pressure gradient to deduce u_τ, they actually deduced it by fitting the near-wall data to the required $U^+ = y^+$ viscous sublayer profile; the resulting u_τ differed from that calculated from the pressure gradient by less than 6%.) The log-linear layer extends quite close to the channel centreline (which, at the different Reynolds numbers, is at different values of y^+). Since the flow is symmetric, there must be a zero velocity gradient at $y = h$, so the log-law region clearly cannot extend quite that far.

In turbulent boundary layers, explored in sections 8.3–8.7, there is usually a much more substantial region above the inertial layer, normally termed the outer layer 'wake' but, as is evident in figure 7.6(a), this region is quite narrow in channels, the excess velocity above the log law is very small and, in those particular experiments, it is only really noticeable at the highest Reynolds number. As far as U^+ is concerned, figure 7.6(a) suggests that Reynolds number effects are weak. Not surprisingly, however, they are not weak when the turbulence statistics are considered. This is most obvious in the shear stress profiles, shown in figure 7.6(b), in which the thickness of the region where viscous stresses are important seems to extend to at

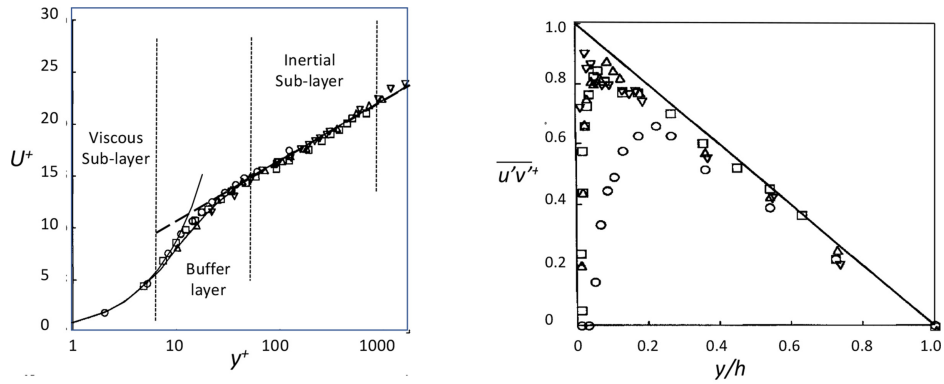

Figure 7.6. Mean velocity (a) and turbulence shear stress (b) profiles in wall units, from a turbulent channel flow, at four Reynolds numbers. $\mathrm{Re}_c(\mathrm{Re}_\tau)\approx$: O, 2970 (170); □, 14914 (710); △, 22776 (1012); ▽, 39582 (1650). Reproduced with permission from [52], copyright Cambridge University Press.

least $y/h = 0.25$ at the lowest Reynolds number. In the course of this experiment, it was shown that there is a significant interaction between the turbulence structures within one half of the channel and those in the other half; this is not surprising, for there is no 'hard' boundary at $y = h$ and eddies from below that point are able, instantaneously, to migrate to the upper half.

High-quality DNS experiments remove the inevitable uncertainties that arise in laboratory work; figure 7.7(a) shows mean velocity profiles obtained during a comprehensive set of computations by Jiménez and his co-workers [14, 15, 21]. At the higher Reynolds numbers in particular, these were expensive computations. For the reader's interest, at $\mathrm{Re}_\tau = 2003$ about 1.7×10^9 grid points were used and 6×10^6 processor hours of a supercomputer system with 2048 processors were required; 25TB of raw data were produced [14]. This kind of computation would have been inconceivable much before the beginning of this century. Except for the lowest Re_τ case, all the velocity profiles seem to collapse until near the channel centreline, just as the laboratory data shown in figure 7.6(a) suggest. However, on this kind of log-linear scale it is always difficult to be certain about the collapse in the inertial layer, and a more revealing test is to plot what is sometimes called the *Kármán measure* or the *diagnostic function*, defined by

$$\Pi = y^+ \frac{\mathrm{d}U^+}{\mathrm{d}y^+}, \tag{7.32}$$

which should equal $1/\kappa$ wherever the mean profile is logarithmic. The same data are plotted in that form in figure 7.7(b), in which it is clear that data at the highest Re_τ (4200) provide a substantial region of constant Π – extending over the approximate range $200 \leqslant y^+ \leqslant 1200$. In that region, its value is 2.58, so that $\kappa = 1/\Pi = 0.387$. The theoretical log-law line plotted in figure 7.7(a) thus uses $\kappa = 0.387$ and $A = 4.5$. This

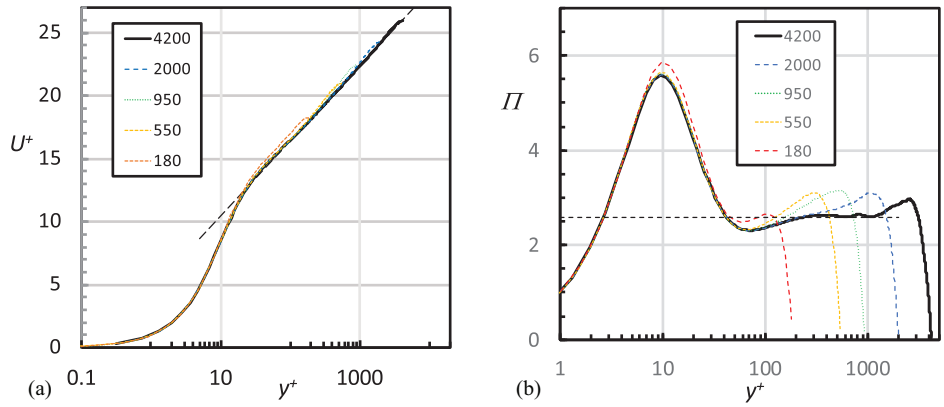

Figure 7.7. Mean velocity (a) and Kármán measure (KM) (b) profiles in wall units from a turbulent channel flow at five Reynolds numbers. Figures based on the data of Jiménez's group[5] [14, 15, 21]. Re_τ values are given in the legends. The dashed black line in (a) is equation (7.27) with $\kappa = 0.387$, $A = 4.5$.

[5] http://torroja.dmt.upm.es/channels

value of κ is some 3%–6% lower than the 'classical' value of 0.4–0.41, which, for most of the 20th century, was the accepted value. The data for $\mathrm{Re}_\tau = 4200$ plotted in the form of figure 7.7(a) also fit very closely to a log-law line for which $\kappa = 0.41$ and $A = 5.2$ (not shown), which illustrates how careful one should be in using such plots to deduce κ. And, we emphasise, this is in the context of knowing the wall friction velocity exactly, as it is obtained from the applied pressure gradient. In the case of external flows, such as boundary layers, the wall stress (and thus u_τ) is rarely known exactly, as we shall see in section 8.3, and this makes it even more difficult to be certain of the value of κ.

Not surprisingly, therefore, there has been some dispute over the years about the precise value of Kármán's constant, κ. Some authors believe it can be flow-dependent. This view has been well argued by Nagib and Chauhan [31], who preferred to call κ a 'coefficient' rather than a constant, but the issue remains somewhat contentious, especially among purists who believe that, in the spirit of von Kármán, it should be a universal constant. See also the discussions by Marusic [24, 25]. We will say a little more about this in our exploration of turbulent boundary layers in section 8.3.

7.3.4 The surface skin friction

Many authors have sought to measure the important skin friction coefficient. Perhaps the first comprehensive set of experiments, which also covered some of the laminar flow regime, was published by Dean [10]; he deduced a correlation for the fully turbulent channel flow which fitted the data reasonably well and is given by

$$C_f = 0.073\mathrm{Re}_b^{-0.25}, \tag{7.33}$$

where Re_b is the Reynolds number based on the bulk velocity and full channel width, $(2hU_b/\nu)$ and $C_f = 2\tau_w/(\rho U_c^2)$, respectively. Figure 7.8 shows this result and an

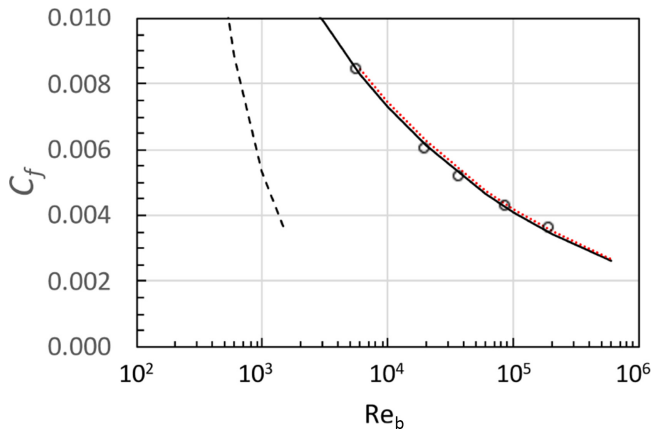

Figure 7.8. Skin friction coefficient in a turbulent channel flow. Symbols are deduced from the data of Jiménez's group[6]; the dashed line is the laminar case ($C_f = 16/(3\mathrm{Re}_b)$); the solid black and dotted red lines are the Dean and Zanoun correlations [10, 56], respectively.

[6] http://torroja.dmt.upm.es/channels

alternative, much later, correlation [56] based partly on more modern, and hence arguably more accurate, experimental techniques. Nonetheless, the difference is very small (0.073 is replaced by 0.0743 in the above equation). The DNS data from which figure 7.7 was derived can also be used to deduce Re_b and C_f, and the results are included in figure 7.8. Recall that transition is normally reckoned to begin at $\mathrm{Re}_b \approx 1500$, so C_f then begins to rise from its laminar value towards the fully turbulent line, and transition is complete by about $\mathrm{Re}_b \approx 3000$. It is also possible to deduce the C_f variation from the defect law for the velocity profile. This requires some straightforward assumptions, but the result is close to the data shown in figure 7.8; the details are given by Pope [36].

7.3.5 The turbulence

DNS computations, unlike laboratory experiments, allow deep exploration of any of the turbulence statistics that may be of interest. We conclude this section with comments about some of these, as deduced from the computations mentioned above by the Jiménez group. Figure 7.9 shows the rms axial velocity fluctuation profiles corresponding to the velocity profiles in figure 7.7(a), plotted against both y/h and y^+. A number of points should be noted. First, recall our comment in the previous section that Couette flow turbulence is noticeably more anisotropic than it is in channel flows. This is evident by comparing figure 7.9(a) with figure 7.4(a). For example, on the centreline ($y/h = 1$), the ratio of the axial to the vertical (or spanwise) rms fluctuations is 1.5, whereas in Couette flow it is between about 1.6 (for $u'^+_{\mathrm{rms}}/w'^+_{\mathrm{rms}}$) and 2.0 (for $u'^+_{\mathrm{rms}}/v'^+_{\mathrm{rms}}$). The ratio increases somewhat as y/h decreases.

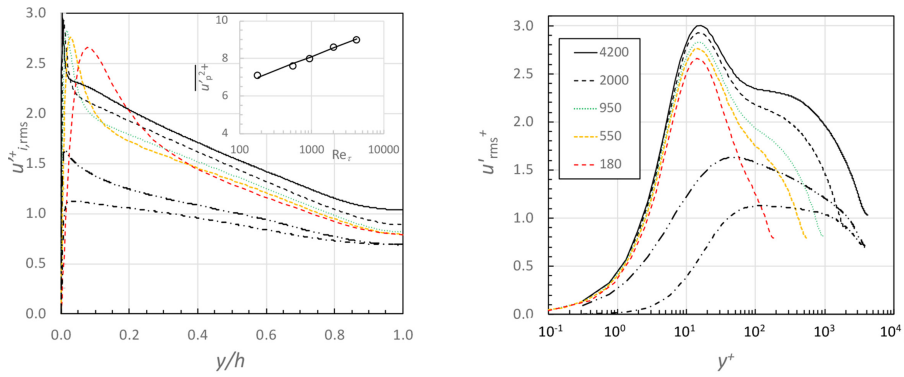

(a) (b)

Figure 7.9. (a) Profiles of the axial velocity intensity profiles (rms values) for a turbulent channel flow at five Reynolds numbers. Figure based on the data of Jiménez's group[7] (as in figures 7.6 and 7.7); Re_τ values are given in the legend of (b). The inset in (a) shows the variation of the peak mean square values as a function of Re_τ, fitted by $\overline{u'^2}^+_p = 0.65\ln(Re_\tau) + 3.65$. The lower two (black) lines are profiles of v'^+_{rms} (the lowest line) and w'^+_{rms}. (b) The same as in (a), but plotted against y^+.

[7] https://torroja.dmt.upm.es/channels/data/statistics

Second, despite a reasonable collapse in the mean velocity profiles over the Reynolds number range studied (see figure 7.7(a)), there is clearly no collapse in the $u'^{+}_{i,\,\mathrm{rms}}$ profiles however they are plotted. The fact that fluctuation profiles are not independent of Re_τ, even within the log-law region, suggests that the usual wall scaling is inadequate for the turbulence statistics in the way that is classically expected, no doubt because the influence of the outer layer turbulence extends into the viscous region. There have been a number of attempts to introduce alternative scaling to take account of this, starting with [13], and subsequently, with varying degrees of success. We do not pursue the issue here, although rather more is said about it in section 7.4 because data (for the corresponding pipe flow case) are now available at much higher Reynolds numbers.

Third, it is evident that, as in Couette flow, there are peak values of u'^{+}_{rms} near the wall at a roughly constant $y^+ \approx 15$ – see figure 7.9(b). This peak value increases with the Reynolds number and, as shown in the inset of figure 7.9(a), its mean square value varies logarithmically, at least over this range of Re. Such a variation was first noted in the laboratory in the context of boundary layers by De Graaff and Eaton [13] but, since the peak is so near the wall, its accurate measurement is not without difficulty. Quality DNS avoids this difficulty, and the solid line shown in the inset is the fit proposed by the Jiménez group [42], according to the general proposal for the peak variance:

$$\overline{u'^2}^{+}_{p} = A \ln(\mathrm{Re}_\tau) + B, \tag{7.34}$$

which has been much discussed (e.g. [26]) and initially proposed by Townsend [49]. (Note that A and B here are not related in any way to those in the standard log laws, equations (7.28) and (7.31).) It must be emphasised that this behaviour cannot continue as $\mathrm{Re}\rightarrow\infty$, for that would seem to imply asymptotically infinite dissipation in the wall region, as argued by Chen *et al* [9].

We conclude by considering the turbulence kinetic energy (TKE) balance, which we call B_k here. This is exactly the same as in Couette flow, equation (7.11), and was discussed in that context there. We can summarise the full TKE (for a steady flow) as

$$B_k = P_k + T_k + Pr_t + V_k + \epsilon = 0 \tag{7.35}$$

where P_k is the production term, T_k is the turbulent transport, Pr_t is the pressure transport, V_k is the viscous diffusion, and ϵ is the dissipation. These correspond to the four terms in equation (7.11), plus V_k. Recall that we previously ignored this latter term, viscous diffusion, which we include here and which becomes, in this case, $V_k = \nu((\mathrm{d}^2/\mathrm{d}y^2)(k + \overline{v'^2}))$; if the Reynolds number is high, we expect this to be negligible everywhere except close to the wall. In an ideal logarithmic layer in which we expect the Reynolds shear stress to be u_τ^2 (see section 8.3.2) and the mean velocity gradient to be simply $1/\kappa y$, the production term P_k would be $u_\tau^3/\kappa y$, so all the terms in the TKE might be expected to decrease roughly according to $1/y$ away from the wall, which means that an appropriate way to normalise all the terms is to multiply them by y/u_τ^3, as is done for the TKE balance shown in figure 7.10. With a logarithmic scale for y, the areas under each line are then proportional to the total (integrated) energy.

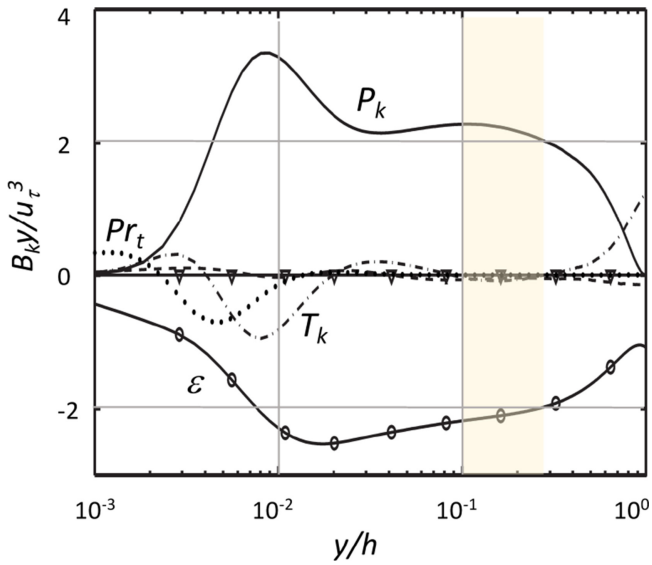

Figure 7.10. Turbulent kinetic energy balance for a turbulent channel flow, with each term normalised using y and u_τ^3: $B_k y/u_\tau^3$. The yellow region marks the approximate extent of the mean velocity log law. The data correspond to the results shown in figures 7.6 and 7.8 for the $\mathrm{Re}_\tau = 2000$ case[8].

According to the data in figure 7.7(b), the buffer layer extends up to about $y^+ = 50$, i.e. $y/h \approx 0.025$ – beyond that, the Kármán measure Π is constant at $1/\kappa$. Note first from figure 7.10 that energy production roughly balances its dissipation in the region above this buffer layer, defined approximately by $0.025 < y/h < 0.4$. It also shows that the $1/y$ behaviour holds quite well. Above $y/h = 0.4$, the production decreases faster than that, because the mean velocity gradient reduces (and is zero at $y/h = 1.0$, of course). The dissipation then becomes increasingly balanced by turbulent transport (the triple velocity product) as the centreline is approached. Second, below $y/h = 0.025$ (i.e. in the buffer layer and below), viscous diffusion becomes important, as does turbulent transport. In this region, an adequate energy balance thus requires the inclusion of V_k, as seen for Couette flow in the previous section. Just as in the latter flow, energy enters the flow by the action of the mean flow that drives the production of the axial velocity fluctuations (recall equation (7.10) and the surrounding discussion). It is the pressure strain terms that redistribute the energy to the other components (with dissipation then removing energy from all the components).

The various features of the mean velocity and turbulence fields discussed in this and the previous section are similar to those in very many wall-bounded flows, including external flows. There are differences, nonetheless, because external wall flows have additional complicating influences. In particular, in turbulent boundary layers there is always, at the very least, some dependence on x – the flow develops in

[8] Figure reprinted from [15] with the permission of AIP Publishing.

the streamwise direction, so homogeneity in that direction does not usually exist. This is the topic of chapter 8.

7.4 Pipe flows

7.4.1 Introductory matters

Perhaps the most common type of internal turbulent flow worldwide is that in pipes. A straight, smooth-walled pipe (figure 7.11) is the axisymmetric equivalent of the planar channel flow we considered in the previous section. A brief reminder of the laminar case is given first, to set the scene. Consider a straight, smooth-walled pipe of internal diameter d, where d is much smaller than the pipe length. The flow is driven through the pipe by a pressure difference between its ends which, apart from relatively short regions near these ends, leads to a constant pressure gradient equal to $-\mathrm{d}P/\mathrm{d}x$ along the pipe's length (the pressure falls along the pipe). A simple force balance over the entire pipe cross-section leads to an equivalence between this pressure gradient and the frictional stress on the inside wall of the pipe, τ_w, i.e.

$$-\frac{\mathrm{d}P}{\mathrm{d}x} = \frac{4\tau_w}{d}. \tag{7.36}$$

A similar balance can be expressed by equating the force that results from the pressure difference acting on a circular cross-section between the centre of the pipe

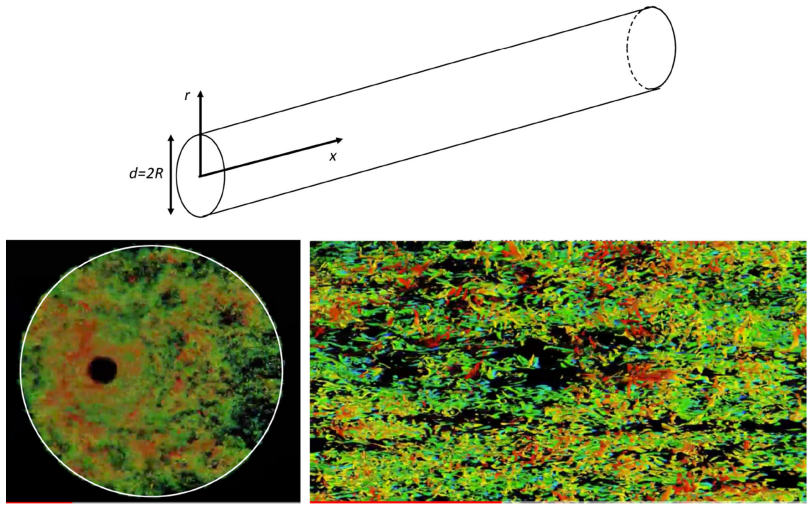

Figure 7.11. Sketch of pipe geometry and snapshots of the vortex structures, from a DNS at Re = 133000, $\mathrm{Re}_\tau = Ru_\tau/\nu = 3008$, from the visualisations by Ahn[9] [1]. The left-hand view is down the length of the pipe along an axis slightly inclined to the pipe's axis (so that the end of the pipe is off-centre). The right-hand view is a streamwise slice through a plane normal to the pipe's axis.

[9] https://gfm.aps.org/meetings/dfd-2015/55f566dc69702d060d510300, copyright (2015) by the American Physical Society.

and an arbitrary radius, r, and that provided by the internal shear stress, τ, acting on the circumference of that section over the pipe length. In the absence of turbulence, only the viscous stress given by $-\mu dU/dr$ (U falls with increasing r), contributes to this internal stress, and integration of the resulting balance leads to the well-known result that the axial velocity profile is parabolic (just as in a planar channel, see figure 7.2) and given by

$$\frac{U}{U_c} = 1 - \left(\frac{r}{R}\right)^2, \tag{7.37}$$

where U_c is the centreline velocity and $R = d/2$ is the pipe radius. The bulk velocity in the pipe, U_B, is easily shown to be one half of U_c. As for the planar channel, the flow Reynolds number can be defined in terms of the bulk velocity: $\mathrm{Re} = U_B d/\nu$. It has been common practice since the Blasius era to define a *friction factor* f as

$$f \equiv -\frac{\mathrm{d}P}{\mathrm{d}x}\frac{d}{\frac{1}{2}\rho U_B^2}, \tag{7.38}$$

which is equal to $4C_f$, with the friction coefficient defined in the usual way ($C_f = 2\tau_w/\rho U_B^2$). Note that equations (7.36) and (7.38) imply that $f = 8(u_\tau/U_B)^2$. Using the velocity profile given by equation (7.37), which is only valid for laminar flow, it is straightforward to show that, in that case, $f = 64/\mathrm{Re}$. Reynolds' early experiments in the 1880s (see section 2.8) suggested that transition to turbulence begins at an Re of around 2000, but even after 140 years there remains much discussion both about the precise values of what are usually called the lower critical Reynolds number (below which turbulence cannot be maintained) and the upper critical Reynolds number (above which laminar flow cannot be maintained). Indeed, Reynolds himself recognised that no unique value delineates the laminar and turbulent states. It is now known that the parabolic velocity profile of equation (7.37) remains linearly stable to infinitesimally small perturbations up to infinite Re, so the value of the upper critical Re can, in fact, be made very high if the natural perturbations in the experiment are sufficiently small.

We do not discuss the fascinating topic of turbulent transition anywhere in this book, but in the context of pipe flows, the interested reader would profit from perusing [30] and Eckhardt's selection of papers [12] published as a thematic volume marking the 125th anniversary of the publication of Reynolds' historic paper, which together cite a small fraction of the thousands of papers which have addressed the topic. It is sufficient to point out, first, that uncertainties remain in trying to assign precise values to both the lower and the upper critical Reynolds numbers but, second, in practically all industrial circumstances, the 'natural' disturbances are sufficiently large and Re sufficiently high to ensure that the flow is fully turbulent. In practice, $\mathrm{Re} \approx 2300$ remains a reasonable value at which the flows in a typical (undergraduate student demonstration) experiment or an industrial gas line, for example, become turbulent. We thus turn to a consideration of fully turbulent pipe flow, recognising that this topic has also attracted huge numbers of researchers and

continues to do so. Figure 7.11 shows snapshots of pipe turbulence, from a video which the reader may like to explore.

7.4.2 The friction factor

Not surprisingly, perhaps, there is an enormous literature on turbulent pipe flows. As in the laminar case, these are in some ways simply the axisymmetric equivalent of turbulent planar channel flows, depending, as they both do, only on the applied axial pressure gradient and a characteristic Reynolds number. However, there are significant differences that arise from the nonzero transverse curvature of the cross-stream coordinate in pipe flows and, consequently, the fact that there are 'side walls' whatever the value of y^+. From a practical perspective, the most important requirement is to know what the friction factor f is for a given Reynolds number (the only parameter on which it depends), for that will determine the power that is necessary to drive the fluid through the pipe. Those familiar with undergraduate texts or, indeed, industrial design codes for pipework, will be aware that for values of Re up to about 10^5, the very early relation of Blasius [6] provides a good fit, even to the subsequent large body of data not then available. Defining f by equation (7.38), his result was

$$f = 0.316/\mathrm{Re}^{1/4}. \tag{7.39}$$

Integrating $2\pi U r \mathrm{d}r$ across the pipe to obtain the bulk velocity U_B in the usual way (replacing r by R and y with y measured from the pipe wall), and using the fact that f can also be written as $8u_\tau^2/U_B^2$ (compare equations (7.36) and (7.38)), leads immediately to

$$\left(\frac{8}{f}\right)^{1/2} = \frac{U_B}{u_\tau} = 2\int_0^1 U^+\left(1 - \frac{y^+}{R^+}\right)\mathrm{d}\left(\frac{y^+}{R^+}\right). \tag{7.40}$$

This shows that the variation of f with Re depends only on the form of the velocity profile. (Note that $\mathrm{Re} = 2(U_B/u_\tau)\mathrm{Re}_\tau$, with $\mathrm{Re}_\tau = Ru_\tau/\nu$.) Blasius deduced equation (7.39) using an assumption of a one-seventh power law for the velocity profile and on the basis of many extant measurements, not least the extraordinarily meticulous data produced by Saph and Schoder [39] in the first decade of the 20th century. (Readers might find a recent historical review of interest in this regard [44].)

For $\mathrm{Re} > 10^5$, the Blasius relation fails to describe the data and another well-known relationship was derived by Prandtl, who assumed a log-law velocity profile. The result is known as *Prandtl's friction law for smooth pipes*; he adjusted the constants slightly so that the relation agreed well with the extant friction factor data obtained by Nikuradse [33]. The result is

$$\frac{1}{\sqrt{f}} = 2.0\log(\mathrm{Re}\sqrt{f}) - 0.8, \tag{7.41}$$

to be compared with Blasius' law and the laminar result, $f = 64/\mathrm{Re}$. Schlichting [41] believed this result to be valid to arbitrarily high Re (and therefore thought that measurements at higher Re were not required!). Figure 7.12 shows the two relations and the laminar flow result, connected by a transitional region (marked in red). The latter should be taken as approximate; whilst there are some extant measurements covering that regime for particular experimental setups, e.g. [40], the significant uncertainties about transition that were mentioned earlier suggest that it would be unwise to attempt precision in this range of Re. Figure 7.11 includes some much more recent data obtained from the *Princeton superpipe* experiments. This facility was specifically designed to achieve very much higher Re than ever before by using highly pressurised air so as to increase its density (and hence Re) by more than an order of magnitude. Although, unlike the Blasius relation, the Prandtl one works well up to nearly 2×10^6, it deviates noticeably from the data beyond that point. Superpipe data for $\mathrm{Re} \geqslant 10^4$ and further careful study [27, 55], led to a modification of the two constants in equation (7.41) from 2.0 and 0.8 to (eventually [28]) 1.93 and 0.537, respectively, providing a good fit over more than a decade of the highest Re as well as for lower Re, as evident in the figure. At the time of writing, therefore, the best attested friction law for turbulent flow in smooth pipes at Re values in the range of $3 \times 10^5 \leqslant \mathrm{Re} \leqslant 3.5 \times 10^7$ is

$$\frac{1}{\sqrt{f}} = 1.930 \log(\mathrm{Re}\sqrt{f}) - 0.537. \tag{7.42}$$

At lower Reynolds numbers (but above the fully developed turbulence state), Prandtl's friction law applies, and the Blasius relation is also adequate at Re values up to $\mathrm{Re} = 10^5$.

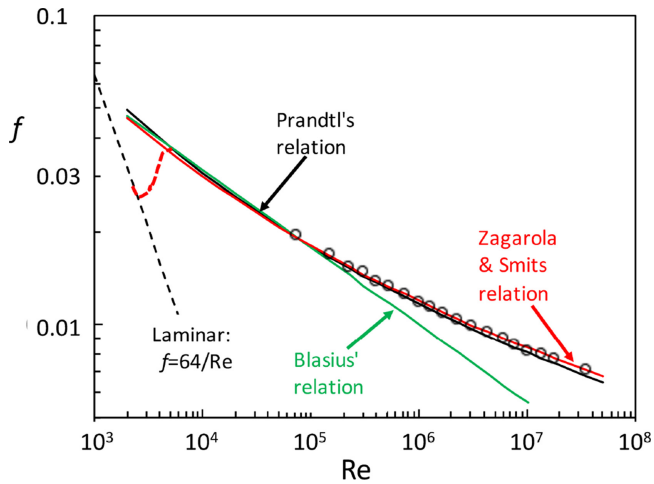

Figure 7.12. Friction factor for pipe flow. The approximate transitional region is shown as a dashed red line, rising up from the laminar result (dashed black line). The other lines are the relations of Blasius, Prandtl, and Zagarola and Smits, equations (7.39), (7.41) and (7.42), respectively. The symbols are data values given by McKeon *et al* [27], obtained in the Princeton superpipe.

The differences between these various relationships essentially result from differences in the assumed velocity profiles. At asymptotically large Reynolds numbers, for which there is sufficient separation in scales between the near-wall viscous-dominated region (where $U^+ = y^+$ with $y = R - r$) and the outer flow, one can deduce the well-known log law in essentially the same way as discussed for channels in section 7.3.2 (and used by Prandtl to obtain his friction law, (equation (7.41)). One of the early findings, however, was that the log-law regime, in terms, say, of its range of y^+ at a given Re, is not as extensive as it is in a channel flow at the same Re, even when this is well above 3000. (Recall from section 7.3.2 that the log law fits the extant channel data very well nearly up to the centre of the channel.) This difference between pipe flows and channel flows was perhaps first noted by Patel and Head [34].

7.4.3 The velocity profile

Figure 7.13 shows a selection of the mean velocity profiles obtained in the Princeton superpipe. These are similar to channel flow profiles (figure 7.7(a)), although in each case there is a more significant ('core') region between the upper end of the log-law range and the pipe centreline. The profiles collapse where they overlap in the log-law y^+ range. Note that the measured profiles extend beyond the centreline, so that the value of U_c^+ for each case can conveniently be deduced as the maximum in the profile. This clearly increases as Re increases, as does the extent of the log-law region.

One expects the existence of the log law to be most likely for higher Reynolds numbers, but a careful inspection of the profiles (not really possible using this figure)

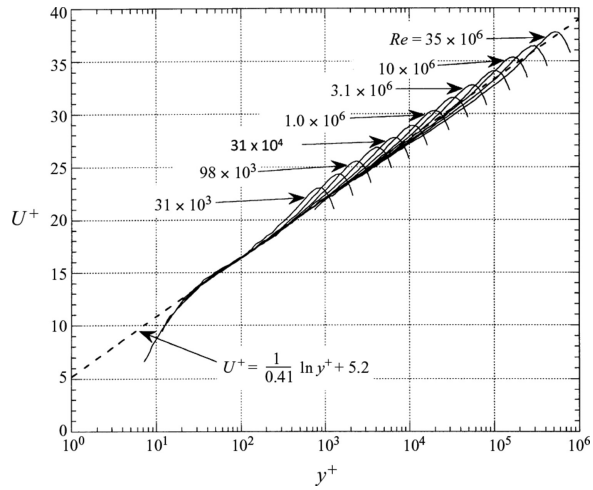

Figure 7.13. Mean velocity profiles obtained in the Princeton superpipe[10]. Reynolds numbers (Re) are shown for alternate profiles and the dashed line is the classical log law with $\kappa = 0.41$ and $A = 5.2$.

[10] Figure reprinted with permission from [55], copyright (1997) by the American Physical Society.

contradicts this, unless the range of the log law is taken to be, say, $600 < y^+ < 0.07\mathrm{Re}_\tau$, which is significantly more restricted than the commonly accepted limits ($50 < y^+ < 0.15\mathrm{Re}_\tau$) [55]. With these more restricted limits, the implication is that the log law cannot exist for $\mathrm{Re}_\tau < 600/0.07 = 8571$, which corresponds roughly to $\mathrm{Re} < 4 \times 10^5$. In that range, provided that Re is large enough to ensure an overlap between inner and outer regions, it turns out that a power law gives a better fit to the velocity profile, as found in the $\mathrm{Re} = 44000$ DNS of Wu and Moin [53], for example. (This is consistent with the Blasius frictional law, since he assumed a power law.) It has therefore been argued that pipe flow velocity profiles actually have a three-layer structure, in which the classic log law emerges at high enough values of Re_τ, but above a power-law region which is always present just above the near-wall viscous layer [11]. This latter work provides a useful entry to the literature on the nature of pipe flow velocity profiles.

Incidentally, the value of the Kármán coefficient κ is about 0.41 for good log-law fits to the profiles in figure 7.13, and this value was also found to be consistent with the implications of the centreline velocity data [28]. It is noticeably different from the value for channel flows (0.387, see section 7.3) and this issue will be discussed further in section 8.3.2. It is also worth noting that direct numerical simulations have begun to reach at least moderately high values of Re. Computations are now available at $\mathrm{Re} = 44000$ [53], which is higher than the lower end of the superpipe range of cases but still significantly lower than the highest Reynolds numbers reached experimentally at the Princeton superpipe facility. These produce data that agree with the superpipe results at the same Reynolds number and yield a power law for the velocity profile, in agreement with the Princeton findings. One can expect computations at significantly higher Re values in the future, to match the largest ones obtainable in the specialist laboratory facilities typified by the Princeton superpipe. Such computations avoid, among other things, the uncertainty about the development length that is needed in a laboratory facility for fully developed conditions to be reached. This has been a contentious issue, but there is some evidence that at least $80d$ is necessary before the turbulence statistics become invariant with downstream distance, significantly less than seems to be required for planar channels; see the discussion by Marusic *et al* [24] and the references therein.

7.4.4 The turbulence

It remains to make a few comments about the fully developed turbulence statistics. Recall first that the mean velocity profiles in pipes and channels are somewhat different, not least because there is a more noticeable outer layer wake component in the pipe flow case (see figures 7.7(a) and 7.13), which was actually noted as early as the 1960s [34]. Nonetheless, more recent studies (e.g. [32]) making explicit comparisons of, for example, the Reynolds stress profiles at the same Re in pipes and channels, have indicated that despite the differences in mean velocity profiles, the stresses are very similar all across the flow – not just in the inertial layer. In the inner region, the peak axial turbulence stress rises slowly with Re in both pipes and channels (recall the channel case shown in figure 7.9(a)) and note that, anticipating

our boundary layer discussion in section 8.3, the same happens in smooth wall boundary layers. However, it is perhaps currently unwise to be too dogmatic about this rise, and particularly whether or not it occurs up to the highest Re currently achieved in laboratories, given the extreme difficulty in making accurate measurements so near the wall (around $y^+ = 15$). There seems to be some evidence that it does not [16, 51].

At a sufficiently high Reynolds number, an outer peak in $\overline{u'^2}^+$ also appears, as illustrated in figure 7.14, which shows the $\overline{u'^2}^+$ profiles for a range of Re from about 2000 up to 98000, corresponding to a Re range of around 8×10^4 up to 6×10^6. A feature of these profiles is that, at least for the higher Re, the stress seems to fall logarithmically in the outer region. In fact, it was suggested long ago [49], on the basis of arguments related to those that lead to the log law in the mean velocity, that streamwise and spanwise velocity fluctuations would display a similar log law so that, for example,

$$\overline{u'^2}^+ = B_1 - A_1 \ln \frac{y}{R}. \tag{7.43}$$

It was later demonstrated that such behaviour could be derived by building on Townsend's *attached eddy hypothesis* (see section 8.5) and considering the spectral content of the fluctuation field [35]. Considerable attention has been paid to this suggestion; some data sets are in apparent conformity with the logarithmic behaviour, but others are not (in the context of boundary layers as well as channels

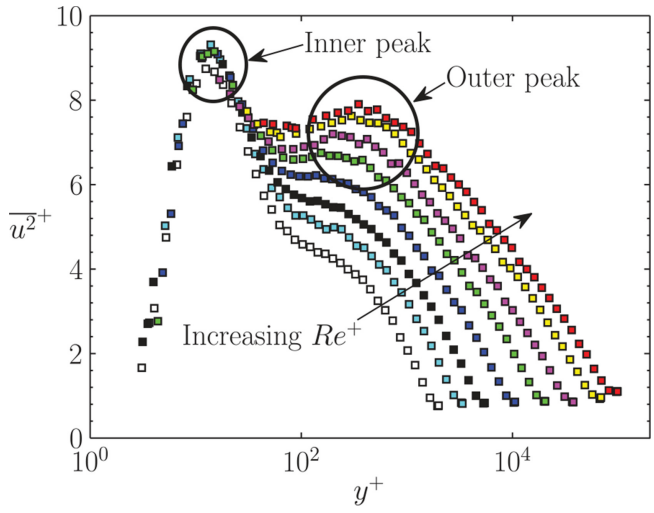

Figure 7.14. Axial Reynolds stress profiles for Re_τ values from 1985 to 98187. Princeton superpipe data[11].

[11] Figure reprinted with permission from [16], copyright (2012) by the American Physical Society.

and pipes). More recently, it has become apparent that only for Re_τ in excess of about 20000 can one really expect to see an extended region of such behaviour, which occurs over the same inertial range (in y^+) in which the mean flow log law applies, e.g. [51]. We discuss all this further in the context of boundary layers in section 8.3. Note finally that the similarity in stress profiles for pipes and channels also holds for the various spectra of the fluctuating velocity (and pressure); see [29], for example. Given the similarities in the stresses, similarities in the spectra are arguably not too surprising, although boundary layer spectral data are nonetheless rather different; see section 8.4.

We have thus far made no comments about the *dynamical* features of these various internal flows, but have merely presented time-averaged quantities. However, it should be obvious that these time averages, as in any turbulent flow, must depend on the nature of the structural features of the turbulence, whether those are near the wall, within the inertial layer, or in the outer region. This whole issue is discussed in the context of boundary layers in section 8.5, where we comment on the extent to which the general features differ between internal and external flows. It is worth saying here, however, that most of the important features do not differ very markedly.

7.5 Subject giant: G I Taylor

Sir Geoffrey Ingram Taylor (7 March 1886–27 June 1975) was a true giant of the field, having had a distinguished career as an English physicist and mathematician at the University of Cambridge for over 60 years. He was described in his obituary by Sir Brian Pippard as follows (quoted in [43]):

> 'Sir Geoffrey Ingram Taylor, who died at the age of 89, was one of the great scientists of our time and perhaps the last representative of that school of thought that includes Kelvin, Maxwell and Rayleigh, who were physicists, applied mathematicians and engineers – the distinction is irrelevant because their skill knew no such boundaries. Between 1909 and 1973 he published voluminously, and in a lifetime devoted to research left his mark on every subject he touched and on every one of his colleagues … his outgoing manner and complete lack of pomposity conveyed, as no formal exposition could have done, the enthusiasm and intuitive understanding that informed all his work.'

Taylor was active in the field of turbulence, having multiple phenomena and concepts named after him, including the Taylor microscale, Taylor's frozen-flow hypothesis, and Taylor dispersion (in pipe flow and elsewhere), to name a few, all of which we touch upon in this text. His research spanned both fluid and solid mechanics and he published widely over his more than 60 years of a dedicated research career; his first paper appeared during his undergraduate years, studying the interference fringes formed by light waves (1909), and the last (at the age of 83), was on thunderstorms. During the First World War he contributed to the war effort, working for the Royal Flying Corps at Farnborough and helping to design and

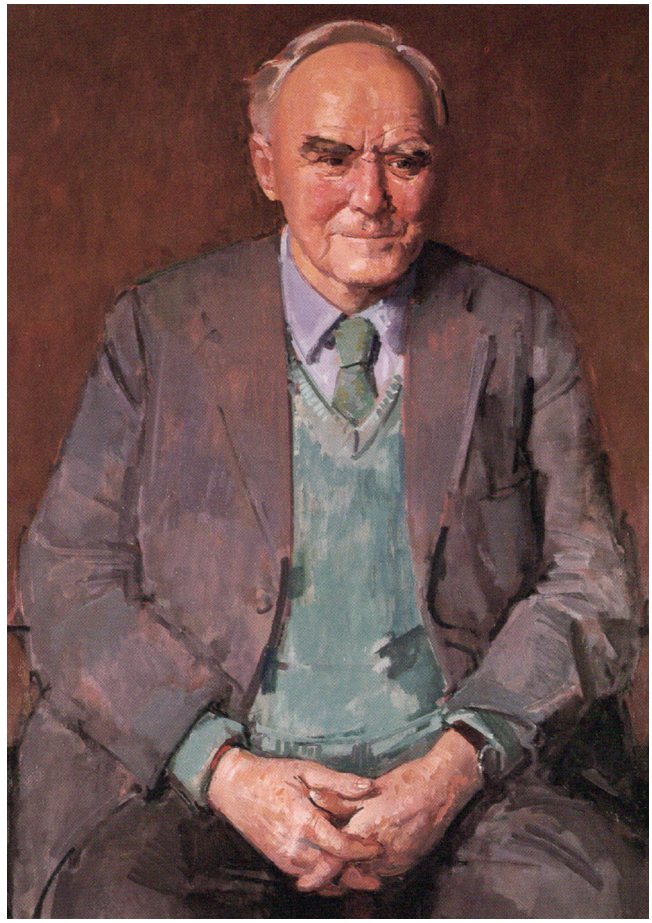

Figure 7.15. Portrait of Sir Geoffrey Ingram Taylor (7 March 1886–27 June 1975). Reproduced with permission from [4], copyright Cambridge University Press.

improve the operation of aircraft. He also made significant contributions during the Second World War, being called upon to be part of the British delegation to the Manhattan Project. It was during this war, in 1944, that he received his knighthood.

Taylor corresponded with and influenced many of the other notable researchers in turbulence of the time including Burgers, Richardson, Prandtl, and von Kármán, notably reflected in the fact that Taylor published a bibliographical memoire of von Kármán following his death. He also left his legacy as the supervisor of both Batchelor and Townsend, who both went on to make substantial contributions of their own to the turbulence field. It was Batchelor who compiled Taylor's entire collected works into four volumes and subsequently wrote a book on *The Life and Legacy of G.I. Taylor* [4]. It is perhaps amusing for modern academics that for almost all of his life at Cambridge, he held research posts and was thus free of

routine teaching, administrative, departmental, or institutional tasks; Rutherford once described Taylor as being 'paid to do no work'. There is an interesting video of G.I. (as he was affectionately known), filmed in 1967, in which he discusses low Reynolds number flow; it is part of the National Committee for Fluid Mechanics Films (NCFMF)[12].

Sample exercises

7.1. Derive the total stress equation for Couette flow given by equation (7.2) from the x-direction mean momentum equation. Are there any other flows for which this would also be valid?

7.2. Assuming that turbulent Couette flow has an S-shaped velocity profile as sketched in figure 7.2, sketch the expected shapes of the viscous stress (i.e. $\mu dU/dy$), the turbulent stress (i.e. $\rho\overline{u'v'}$), and the total stress (i.e. τ) profiles over $0 < y/h < 2$. Compare your sketches with the results presented in figure 7.3.

7.3. For a turbulent channel flow, sketch the expected shapes of the viscous stress (i.e. $\mu dU/dy$), the turbulent stress (i.e. $\rho\overline{u'v'}$), and the total stress (i.e. τ) profiles over $0 < y/h < 2$. Contrast these with those for Couette flow from the previous exercise.

7.4. The file 'ChannelData.txt'[13] contains the velocity profile within channel flow at $Re_\tau = 2000$ by Hoyas and Jiménez [14]. This exercise explores how the velocity profile compares with the expected linear relationship in the viscous sublayer and the logarithmic relationship in the inertial sublayer.

(a) Plot the velocity profile U^+ versus y^+ using linear axes. Zoom in to the near-wall region and compare the profile with $U^+ = y^+$, which is expected in the viscous sublayer. Over what range of y^+ is this valid?

(b) Zoom out and adjust the axes to display this plot of U^+ versus y^+ using log-linear axes. Fit the log law, equation (7.28), using $\kappa = 0.387$ and $A = 4.5$.

(c) Plot the Kármán measure Π (given by equation (7.32)) versus y^+. Confirm the approximate extent of the inertial sublayer and the value of $1/\kappa$ indicated by the plateau.

7.5. The file 'PipeData.txt'[14] contains velocity data for a pipe flow at $Re = 10^6$ from the Princeton Superpipe by Zagarola and Smits [54]. This exercise explores how the velocity profile compares with the expected logarithmic and power law profiles.

(a) Plot the velocity profile U^+ versus y^+ using linear axes. Zoom in to the near-wall region and compare the profile with $U^+ = y^+$, which we expect to see in the viscous sublayer. Based on the location of the closest measurement to the wall, estimate the extent (in physical units) of the viscous sublayer in this experiment.

[12] http://web.mit.edu/hml/ncfmf.html
[13] https://github.com/cvanderwel/TurbulentFlows/blob/main/data/ChannelData.txt
[14] https://github.com/cvanderwel/TurbulentFlows/blob/main/data/PipeData.txt

(b) Zoom out and adjust the axes to display this plot of U^+ versus y^+ using log-linear axes. Fit the log law, equation (7.28), using $\kappa = 0.41$ and $A = 5.2$.

(c) Adjust the axes to log-log scaling and consider whether a power law of the form $U^+ = C(y^+)^\gamma$ provides a better fit to the data in the near-wall overlap layer.

References

[1] Ahn J, Lee J H, Lee J, Kang J and Sung H J 2015 Direct numerical simulation of a 30R long turbulent pipe flow at $Re_\tau = 3008$ *Phys. Fluids* **27** 1–14

[2] Avsarkisov V, Hoyas S, Overlack M and Garcia-Galache J 2014 Turbulent plane Couette flow at moderately high Reynolds number *J. Fluid Mech.* **751** R1–1-R1-10

[3] Aydin E M and Leutheusser H J 1987 Experimental investigation of turbulent plane-Couette flow *Proceedings (A88-14124 03-34) Forum on Turbulent Flows (Cincinnati, OH, June 14-17, 1987)* (New York: American Society of Mechanical Engineers) 51–4

[4] Batchelor G and Taylor G I 1996 *The Life and Legacy of GI Taylor* (Cambridge University Press: Cambridge)

[5] Bech K, Tillmark N, Alfredsson P and Andersson H 1995 An investigation of plane turbulent Couette flow at low Reynolds numbers *J. Fluid Mech.* **286** 291–325

[6] Blasius H 1913 Das Aehnlichkeitsgesetz bei Reibungsvorgängen in Flüssigkeiten *Mitteilungen über Forschungsarbeiten auf dem Gebiete des Ingenieurwesens* (Berlin, Heidelburg: Springer) 1–41978-3-662-02239-9

[7] Buschmann M and el Hak M G 2003 Generalized logarithmic law and its consequences *AIAA J* **41** 565–72

[8] Busse F 1970 Bounds for turbulent shear flow *J. Fluid Mech.* **41** 219–40

[9] Chen X, Katepalli R and Sreenivasan R 2021 Reynolds number scaling of the peak turbulence intensity in wall flows *J. Fluid Mech.* **908** 1–11

[10] Dean R 1978 Reynolds number dependence on skin friction and other bulk flow variables in two-dimensional rectangular duct flow *J. Fluids Eng.* **100** 215–3

[11] Diwan S S and Morrison J M 2021 Intermediate scaling and logarithmic invariance in turbulent pipe flow *J. Fluid Mech.* **913** R1–12

[12] Eckhardt B 2009 Turbulence transition in pipe flow: 125th anniversary of the publication of Reynolds' paper *Phil. Trans. R. Soc.* A **367** Theme Issue

[13] Graaff D D and Eaton J 2000 Reynolds-number scaling of the flat plate turbulent boundary layer *J. Fluid Mech.* **422** 319–46

[14] Hoyas S and Jiménez J 2006 Scaling of the velocity fluctuations in turbulent channels up to $Re_\tau = 2003$ *Phys. Fluids* **18** 1–4

[15] Hoyas S and Jiménez J 2008 Reynolds number effects on the Reynolds-stress budgets in turbulent channels *Phys. Fluids* **20** 1–8

[16] Hultmark M, Vallikivi M, Bailey S and Smits A 2012 Turbulent pipe flow at extreme Reynolds numbers *Phys. Rev. Lett.* **108** 1–5

[17] Kitoh O, Nakabyashi K and Nishimura F 2005 Experimental study on mean velocity and turbulence characteristics of plane Couette flow: low-Reynolds-number effects and large longitudinal vortical structure *J. Fluid Mech.* **539** 199–227

[18] Komminaho J, Lundblach A and Johansson A 1996 Very large structures in plane Coutte flow *J. Fluid Mech.* **320** 259–85

[19] Krank B, Fehn N, Wall W A and Kronbichler M 2017 A high-order semi-explicit discontinuous Galerkin solver for 3D incompressible flow with application to DNS and LES of turbulent channel flow *J. Comput. Phys.* **348** 634–59
[20] Laufer J 1950 *Investigations of turbulent flow in a two-dimensional channel* California Institute of Technology 10.7907/6ZYC-HJ88
[21] Lozano-Duran A and Jiménez J 2014 Effect of the computational domain on direct simulations of turbulent channels up to $Re_\tau = 4200$ *Phys. Fluids* **26** 1–7
[22] Lund K and Bush W 1980 Asymptotic analysis of plane turbulent couette-poiseuille flows *J. Fluid Mech.* **96** 81–104
[23] Mansour N, Kim J and Moin P 1988 Reynolds stress and dissipation-rate budgets in a turbulent channel flow *J. Fluid Mech.* **194** 15–44
[24] Marusic I, McKeon B J, Monkewitz P A, Nagib H M, Smits A J and Sreenivasan K R 2010 Wall-bounded turbulent flows at high Reynolds numbers: Recent advances and key issues *Phys. Fluids* **22** 103
[25] Marusic I, JPMonty, Hultmark M and Smits A 2013 On the logarithmic region in wall turbulence *J. Fluid Mech.* **716** 1–11
[26] Marusic I, Baars W and Hutchins N 2017 Scaling of the streamwise turbulence intensity in the context of inner-outer interactions in wall turbulence *Phys. Rev. Fluids* **2** 1–22
[27] McKeon B, Li J, Jiang W, Morrison J and Smits A 2004 Further observations on the mean velocity distribution in fully developed pipe flow *J. Fluid Mech.* **501** 135–47
[28] McKeon B, Zagarola M and Smits A 2005 A new friction factor relationship for fully developed pipe flow *J. Fluid Mech.* **538** 429–43
[29] Monty J, Hutchins N, Ng H, Marusic I and Chong M 2009 A comparison of turbulent pipe, channel and boundary layers *J. Fluid Mech.* **632** 432–42
[30] Mullin T 2011 Experimental studies of transition to turbulence in a pipe *Annu Rev Fluid Mech* **43** 1–24
[31] Nagib H and Chauhan K 2008 Variations of von Kármán coefficient in canonical flows *Phys. Fluids* **20** 101518
[32] Ng H, Monty J, Hutchins N, Chong M and Marusic I 2011 Comparison of turbulent channel and pipe flows with varying Reynolds number *Exp. Fluids* **51** 1261–81
[33] Nikuradse J 1932 Strömungsgesetze in rauhen Rohren *Forschung auf dem Gebiete des Ingenieurwesens* Supplement **4**(B) (English Transl. NACA TT F-10, 359) VDI research booklet 361. Supplement to Research on the Areas of Engineering Issue B Volume 4
[34] Patel V and Head M 1969 Some observations on skin friction and velocity profiles in fully developed pipe and channel flows *J. Fluid Mech.* **38** 181–201
[35] Perry A, Henbest S and Chong M 1986 A theoretical and experimental study of wall turbulence *J. Fluid Mech.* **165** 163–99
[36] Pope S B 2000 *Turbulent Flows* (Cambridge: Cambridge University Press)
[37] Prandtl L 1925 Bericht über die Entstehung der Turbulenz *Z. Angew Math. Mech.* **5** 136–9
[38] Reichardt H 1956 Über die Geschwindigkeitsverteilung in einer geradlinigen turbulenten Couetteströmung *Z. Agnew Math. Mech.* **36** 26–9
[39] Saph A and Scoder E 1903 An experimental study of the resistances to the flow of water in pipes *Trans. Am. Soc. Civ. Eng.* **51** 253–312
[40] Schlichting H 1979 *Boundary Layer Theory* 7th edn (New York: McGraw-Hill)
[41] Schlichting H 1987 *Boundary Layer Theory* (New York: McGraw-Hill)

[42] Sillero J, Jiménez J and Moser R 2013 One-point statistics for turbulent wall-bounded flows at Reynolds numbers up to $\delta^+ \approx 2000$ *Phys. Fluids* **25** 1–15
[43] Sreenivasan K 2011 G.I. Taylor: The inspiration behind the Cambridge school *A Voyage Through Turbulence* ed P A Davidson, Y Kaneda, K Moffatt and K R Sreenivasan (Cambridge: Cambridge University Press) pp 127–86
[44] Steen P and Brutsaert W 2017 Saph and Schoder and friction law of Blasius *Annu. Rev. Fluid Mech.* **49** 575–82
[45] Taylor G 1923 Stability of a vicous liquid contained between two rotating cylinders *Phil. Trans. R. Soc.* A **223** 289–343
[46] Taylor G 1936 Fluid friction between rotating cylinders. II. Distribution of velocity between rotating cylinders when outer one is rotating and the inner one is at rest *Proc. R. Soc. Lond.* A **157** 565–78
[47] Tillmark N and Alfredsson P 1992 Experiments in transition in plane Couette flow *J. Fluid Mech.* **235** 89–102
[48] Tillmark N and Alfredsson P 1998 Large scale structures in turbulent plane Couette flow *Advances in Turbulence VII* vol 46 ed U Frisch (Dordrecht: Kluwer) pp 59–62
[49] Townsend A A 1976 *Structure of Turbulent Shear Flow* 2nd edn (Cambridge: Cambridge University Press)
[50] Tsukahara T, Kawamura H and Shingai K 2006 DNS of turbulent Couette flow with emphasis on the large-scale structure in the core region *J. Turbul.* **7** 1–16
[51] Vallikivi M, Hultmark M and Smits A 2015 Turbulent boundary layer statistics at very high Reynolds number *J. Fluid Mech.* **779** 371–89
[52] Wei T and Willmarth W 1989 Reynolds-number effects on the structure of turbulent channel flow *J. Fluid Mech.* **204** 57–95
[53] Wu X and Moin P 2008 A direct numerical simulation study on the mean velocity characteristics in turbulent pipe flow *J. Fluid Mech.* **608** 81–112
[54] Zagarola M and Smits A 1997 Scaling of the mean velocity profile for turbulent pipe flow *Phys. Rev. Lett.* **78** 239
[55] Zagarola M and Smits A 1998 Mean-flow scaling of turbulent pipe flow *J. Fluid Mech.* **373** 33–79
[56] Zanoun E-S, Nagib H and Durst F 2009 Refined c_f relation for turbulent channels and consequence for high-Re experiments *Fluid Dyn. Res.* **41** 1–12